20

$Ba_{1-X}Sr_XTiO_3$ Ceramics Synthesized by an Alternative Solid-State Reaction Route

R.A. Vargas-Ortíz, F.J. Espinoza-Beltrán and J. Muñoz-Saldaña
Centro de Investigación y de Estudios Avanzados del IPN,
Unidad Querétaro, Libramiento Norponiente No. 2000,
Fracc. Real de Juriquilla, CP Querétaro, Qro.
México

1. Introduction

All materials respond to stimulus, whether it be an electric field, mechanical stress, heat or light. The manner and degree to which they respond varies and is often what determines which material is selected for a given application. On the most basic level, elastic materials deform in response to mechanical stress and return to their original form when the load is removed. Other materials conduct electricity in response to an applied voltage. Both of these are well-known phenomena, and materials with such behaviors are sometimes called "trivial". On the other hand are pyroelectric and piezoelectric materials, which generate an electric field with a stimulus of heat or mechanical stress, respectively (unexpected phenomenon) and are called "smart" or "functional" materials. Ferroelectric materials are materials that exhibit piezoelectricity and pyroelectricity, as well as the phenomenon which gives them their name (ferroelectricity).

Due to their unique properties, ferroelectric materials are widely used in all areas of electronics and microelectronics, such as cellular phones, computers, cars, airplanes and satellites [KENJI, BUCHANAN]. They have a high discharge dielectric constant (ε) [SHEPARD, RADHESHYAM ,ZHIN], which allows them to be used in high permitivity dielectric devices. Their pyroelectric behaviour is used in heat sensors [PADMAJA, YOO, WHATMORE], and their piezoelectricity is applied in devices like resonadores, sonars, horns, and actuators [GURURAJA, YAMASHITA 1997, YAMASHITA 1998, CHEN]. A combination of their properites are applied in electro-optical devices such as controlable diffraction grids, waveguides, etc. [HEIHACHI, HAMMER, BLOMQVIST]. They are also used in dynamic random access memory (DRAM) [KINGON 2000, KINGON 2006, KOTECKI] and non-volatile memory (NVRAM) [MASUI, KOHLSTEDT].

Many "novel" materials known today were developed many decades ago. Ferroelectric materials are no exception, having been discovered more than seven decades ago. Valasek reported the first ferroelectric material, Rochelle salt (potassium or sodium tetrahydrate tartatre, $KNaC_4H_4O_6 \bullet 4H_2O$) in 1921 [VALASEK]. Subsequently, potassium dihydrogen phosphate (KH_2PO_4) was identified by Busch and Scherrer in 1935 [BUSCH], and barium titanate ($BaTiO_3$ or BT) was noted for its unusual dielectric properties by Wainer and

Salomon in 1942-43 [WAINER]. The discovery of ferroelectricity in ceramics from the BaO-TiO_2 system was extremely important, as it was the first ferroelastic made from simple oxide materials. Since the discovery of $BaTiO_3$, several other oxide-based ferroelectric materials have been developed, such as strontium titanate ($SrTiO_3$ or ST), lead zirconate titanate (PZT), lead titanate ($PbTiO_3$, PT), lithium tantalate ($LiTaO_3$) phosphate, and potassium titanyl ($KTiOPO_4$) to name a few [MESCHKE, KUGEL, HIDAKA, GOPALAN, ROSENMAN]. The study of BT-based ceramics with stoichiometric compositions different from pure BT has become one of the most important subjects of ferroelectrics in recent years. Particularly, substitution of Sr^{2+} ions in place of Ba^{2+} ions into BT leads to a solid solution, barium strontium titanate (BSTx or $Ba_{(1-X)}Sr_XTiO_3$, where $0 \leq X \leq 1$). Ferroelectric materials have been synthesized by various techniques, the most commonly used today being the technical or sol-gel process for the production of powders or thin films [BOLAND, PARK, ZHU, KAMALASANAN]. Another technique used to obtain powders is hydrothermal process [XU, RAZAK, VOLD, CHENG]. Finally there is the conventional route solid-state reaction of mixed oxides [VITTAYAKORN, IANCULESCU, CHAISAN] to obtain powders and solid ceramics. The interest of processing highly dense BSTx ceramics is that the Curie temperature and thus the dielectric properties can be tuned using the chemical variations between $SrTiO_3$ and $BaTiO_3$ [BERBECARU, YUN].

This chapter provides the description of an alternative solid-state reaction route based on high energy ball milling and subsequent sintering for the synthesis and densification of BSTx bulk ceramics. It provides a more direct route than the conventional route of mixed oxides. In addition to presenting structural characterization and results of electrical measurements (dielectric constant versus temperature curves and ferroelectric hysteresis loops), a novel technique known as contact resonance piezoresponse force microscopy (CR-PFM) is applied in the detection and characterization of ferroelectric domains in the BSTx samples.

2. Experimental procedures

Titanium oxide (TiO_2 - 99.9% purity, anatase phase, Aldrich), barium carbonate ($BaCO_3$ - 99.9% purity, Aldrich) and strontium carbonate ($SrCO_3$ - 99.9% purity, Aldrich) powders were weighed according to the stoichiometric proportion of Equation 1. The mixture was ball-milled in a high energy vibratory mill (SPEX 8000) for 6 h using a nylamid vial with 10 toughened zirconia balls (10 mm diameter) and a ball-to-powder weight-ratio of 10:1. The milled powders were uniaxially pressed in a stainless steel cylindrical die (10 mm inner diameter) using 1 GPa pressure. The green compacts were placed on top of TiO_2 substrates inside alumina crucibles (to avoid the reaction of barium oxide with the crucibles) and reactively sintered using a two-step heating program (Figure 1). The compacts are heated from room temperature up to 1273 K (reaction temperature) at 5 K/min and held there for 1 h. The temperature is then increased to between 1523 and 1573 K (sintering temperature) at 3.0 K/min and held there for 2 h. Finally they are cooled to room temperature at 3.0 K/min. The resulting BSTx sintered ceramics with the perovskite ABO_3 structure complied with the formula $Ba_{(1-X)}Sr_XTiO_3$ where X = 0, 0.1, 0.2 … 1 and were named accordingly, e.g. BST3 refers to the X = 0.3 composition. The starting powders, milled powders and sintered ceramics were characterized by x-ray diffraction (XRD) using a Rigaku Dmax-2100 diffractometer equipped with Co Kα radiation; scanning electron microscopy (SEM) using a

Philips XL30 ESEM; transmission electron microscopy (TEM) using a JEOL 2010; micro-Raman scattering using a DILOR unit; differential scanning calorimetry (DSC) using a Mettler Toledo; and thermogravimetric analysis (TGA) using a SDTA851 Mettler Toledo. The bulk density of the sintered ceramics was determined using the Archimedes method.

$$(1\text{-}X)BaCO_3 + XSrCO_3 + TiO_2 \rightarrow Ba_{(1-X)}Sr_XTiO_3 + CO_2\ (g) \quad (1)$$

This fabrication method is a modification of the conventional route (solid state reaction) for the manufacture of $Ba_{(1-X)}Sr_XTiO_3$ ceramics. It requires less processing steps (Figure 2), is more straightforward than other chemical processes and, most important, leads to the fabrication of high-density ceramics with very low porosity.

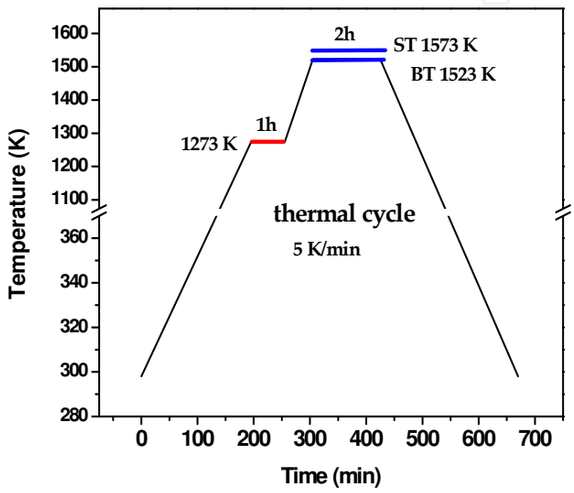

Fig. 1. Heat treatment used for the manufacture of BSTx.

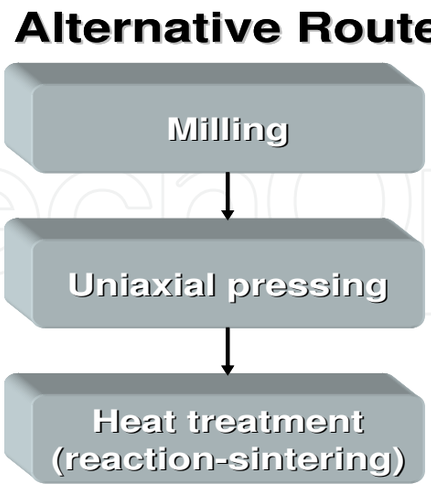

Fig. 2. Stages of the proposed alternative route for the manufacture of BSTx.

It must be noted that the high energy milling process used allows for homogenization and particle size reduction of the starting powders. It is a more efficient process than

conventional attrition, planetarium or automatic-agate milling. The milled powders were compacted using much higher pressure (~1.0 GPa) than applied using the conventional approach (~0.1 GPa). This resulted in uniform green compacts which can conduct an homogeneous chemical reaction. Finally, the thermal treatment induces simultaneous reaction and sintering (reaction-sintering, Figure 1) as opposed to the conventional manufacturing process where the starting powders are milled, thermally-treated to react, a second milling process is performed, and then the twice-milled powders are pressed into compacts. Finally, a second thermal treatment (sintering) densifies the compacts.

3. Results and discussion

3.1 Fabrication of BSTx powders

The high energy milling process significantly affects the size and shape of the starting powders, as seen in the SEM micrographs of Figure 3. Figure 4 shows the TEM micrographs of the starting powders after milling for 6 h. A final particle size of less than 50 nm was attained for both extreme concentrations (only $BaCO_3$ and TiO_2, and only $SrCO_3$ and TiO_2).

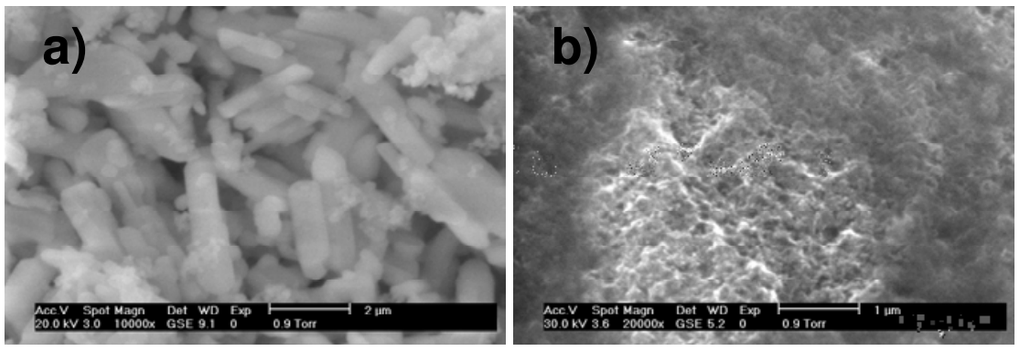

Fig. 3. SEM image of starting powders (a) milled for 6 hours, and (b) before milling.

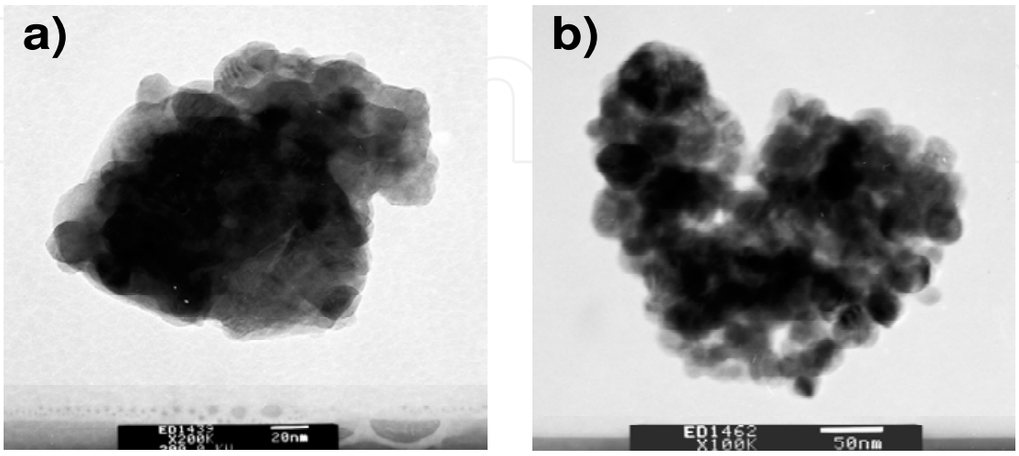

Fig. 4. TEM micrographs of (1-X)$BaCO_3$ + X$SrCO_3$+ TiO_2 powder milled for 6 hours, with (a) X = 0.0 and (b) X = 1.0.

The x-ray diffraction patterns for the milled $BaCO_3$, TiO_2 and $SrCO_3$ powder mixtures are presented in Figure 5. The main $BaCO_3$ peak, located at approximately $2\theta = 28°$ is present up to X = 0.9, and the small peak at approximately 30º belongs to TiO_2. As expected, increasing the $SrCO_3$ content increases the height of the $SrCO_3$ peak located at approximately 30º. There is a degree of amorphization due to the creation of defects in the crystal structure. Figure 6 presents the thermogravimetric analyses (TGA) curves for the same collection of samples as analyzed by x-ray diffraction (Figure 5). All the curves are similar in their key characteristics. The weight loss behavior for a single sample, with X = 0.65, is shown in Figure 8. There are four stages of weight loss centered at 403, 773, 973 and 1273 K. In the first stage, from room temperature (RT) up to 403 K, a weight reduction of approximately 1.3% occurs due to evaporation of water from the material surface. In the second stage, from 403 to 773 K, the weight loss of about 5.2% is related to the loss of chemically bound water in the form of OH groups from the BaOH that was formed when BaO combined with water during milling [BALÁZ]. This loss typically occurs between 473 and 873 K [ASIAIE]. The phenomenon of water loss has also been reported to occur in other carbonates between 593 and 723 K [DING]. The third stage, between 773 and 973 K, is not related to any structural modification of the BSTx samples. According to the literature, the decomposition of strontium and barium carbonates to form CO_2 occurs at higher temperatures, between 1023 and 1273 K [JUDD, L'VOV, MAITRA]. However, in this case, the generation of CO_2 begins as early as at 833 K and runs up to 1273 K. The x-ray difffraction patterns of Figure 7 show the appearance of a peak ($2\theta \approx 36°$) at 873 K, which corresponds to the formation of the perovskite structure of $BaTiO_3/SrTiO_3$. Therefore, the weight loss from 773 to 1323 K can be considered a single stage that varies with Sr content. It is directly related to the CO_2 excess from the carbonates used as starting powders (see Equation 1). It is the difference between the weight of the $(1\text{-}X)BaCO_3 + XSrCO_3 + TiO_2$ starting powders and that of the resulting $Ba_{(1-X)}Sr_XTiO_3$. Table 1 lists the total weight loss, the loss in the different stages, and the weight loss expected from CO_2 liberation. For the group of samples as a whole, an approximate 5% weight loss was observed between RT and 773 K, and the weight loss from 773 to 1323 K corresponds closely to the stoichiometric CO_2 loss.

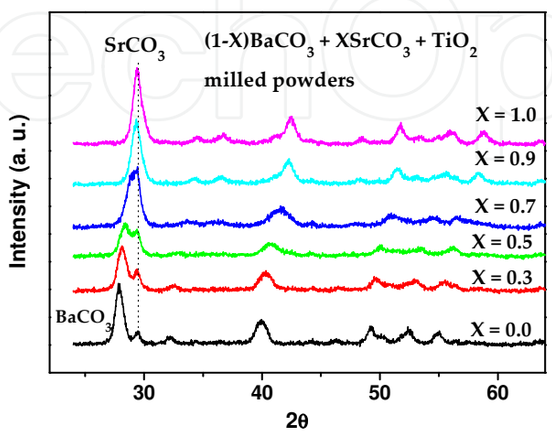

Fig. 5. X-ray diffraction patterns for $(1\text{-}X)BaCO_3 + XSrCO_3 + TiO_2$ milled powders.

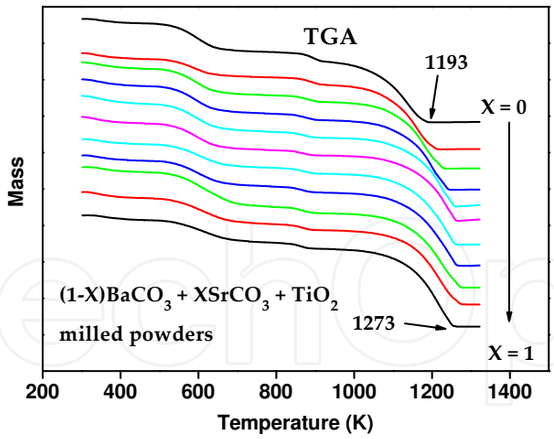

Fig. 6. Thermogravimetric curves of $(1\text{-}X)BaCO_3 + XSrCO_3 + TiO_2$ milled powders.

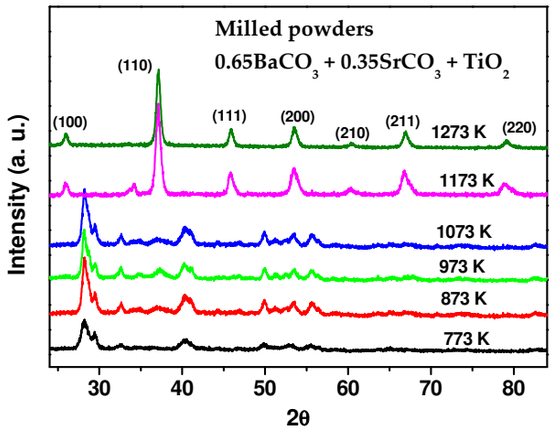

Fig. 7. XRD patterns of $0.65BaCO_3$, $0.35SrCO_3$ and TiO_2 powders milled for 6 hours and subsequently heat treated at different temperatures.

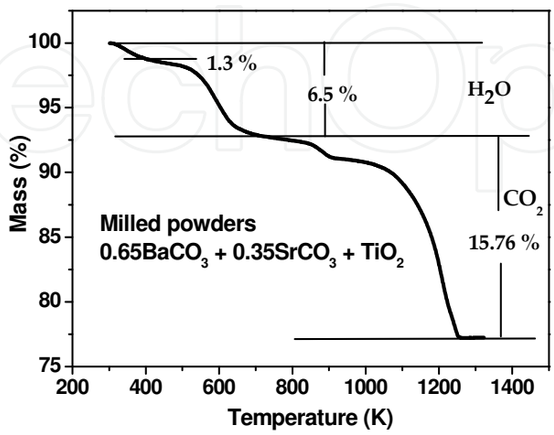

Fig. 8. Thermogravimetric analysis of $0.65BaCO_3$, $0.35SrCO_3$ and TiO_2 powders milled for 6 hours.

The thermogravimetric plots also show a correlation between the Sr content and the temperature at final weight loss (zero slope section). For example, the BST0 sample stops losing weight at around 1193 K but the BST10 (with highest Sr content) at around 1273 K. The temperature at which no more weight loss is observed marks the end of the reaction, as corroborated by the XRD measurements (Figure 7). The thermogravimetric curves can therefore be used as guides to establish the reaction temperature in the BSTx system.

Sample ID	% Total weight loss	% Weight loss from RT to 773 K	% Weight loss from 773 to 1323 K	% Weight loss CO_2 stoichiometric
BST0	20.43	5.56	14.87	15.87
BST1	19.38	4.12	15.26	16.16
BST2	21.02	5.48	15.54	16.47
BST3	21.59	5.61	15.98	16.78
BST4	21.52	5.94	15.58	17.10
BST5	21.39	5.80	15.59	17.44
BST6	21.76	4.85	16.91	17.79
BST7	22.48	5.19	17.29	18.15
BST8	24.29	5.76	18.53	18.53
BST9	23.46	5.42	18.04	18.93
BST10	22.87	4.52	18.35	19.34

Table 1. Thermogravimetric analysis of (1-X)$BaCO_3$ + $XSrCO_3$ + TiO_2 powder after high energy milling for 6 hours.

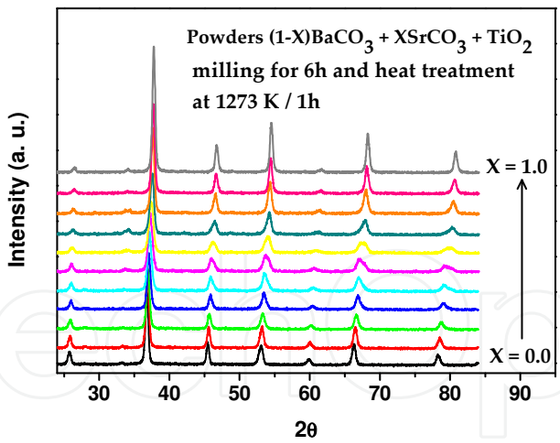

Fig. 9. X-ray diffraction patterns of (1-X)$BaCO_3$ + $XSrCO_3$ + TiO_2 powder milled and heat treated at 1273 K for 1 h. The crystal structure is perovskite-type ABO_3.

The diffraction patterns for the range of samples after milling and thermal treatment at 1273 K for 1 hour are shown in Figure 9. All the samples present the perovskite-type structure ABO_3, indicating the reaction was successfully completed. The formation temperature of the $BaTiO_3$ phase coincides with that reported by L. B. Kong [KONG], where the rutile phase of titanium oxide (TiO_2) was used instead of TiO_2 anatase phase. The peaks shift to higher angle as the Sr content increases. For example, the most intense $BaTiO_3$ peak in Figure 10

shifts from 36.79° for the $BaTiO_3$ (BST0) to 37.77° for $SrTiO_3$ (BST10). This shift corresponds to a reduction in unit cell size, consistent with the difference between the ionic radii of Ba^{2+} (1.34 Å) and Sr^{2+} (1.12 Å). The ABO_3 perovskite structure refers to the relative position of the Ba^{2+}, Sr^{2+} and Ti^{4+} ions with respect to oxygen (O^{2-}). The structure can present as different phases, depending on the material and temperature. For the BSTx system it may be cubic or tetragonal at room temperature, depending on the strontium content. In this case, we observed the cubic phase after 1 hour of heat treatment at 1273 K (Figure 9). The relationship between the cubic and tetragonal phase and the volume of the unit cell will be discussed in more detail when disucssing compaction.

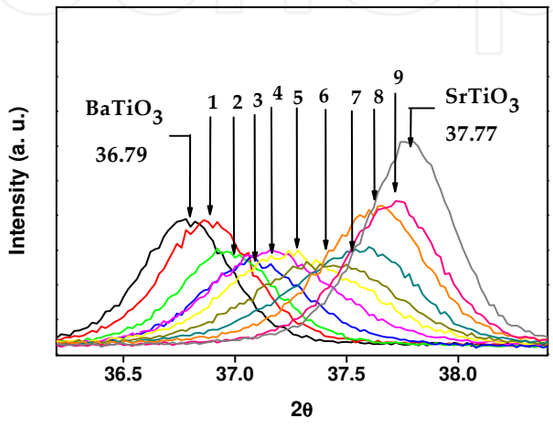

Fig. 10. Expanded view of the primary peak in Figure 9, showing the shift in peak position with increasing Sr content from X = 0 ($BaTiO_3$) to X = 1 ($SrTiO_3$).

3.2 Sintering

During conventional manufacture (solid-state reaction) the starting oxide powders are first milled and calcined. The reacted powders (having the desired stoichiometry) are milled once again to reduce the particle size. They are then compacted into disks or other shapes (green ceramic) and finally, thermally treated to sinter the compact. At the sintering temperature, the ceramic particles coalesce with each other to form grains, the material shrinks and the pores are eliminated [KINGERY]. The alternative manufacturing route of the present work is more straightforward. The starting powders are milled only once to homogeneize and reduce the particle size before being compacted into disks or other shapes. The green ceramics are thermally treated at the reaction temperature (1273 K) to obtain the perovskite-type structure ABO_3. A second heating step is subsequently applied to sinter the ceramic (Figure 1). In this way, dense ceramics (>90% of the theoretical density) are obtained. The sintering temperatures of the samples with intermediate stoichiometry varied between 1523 K for pure $BaTiO_3$ and 1573 K for pure $SrTiO_3$. The temperatures were empirically determined. Such reduced sintering temperatures can only be applied to powders with particle size smaller than 50 nm, which is uniquely attained in our alternative route, thanks to the high energy milling. Whenever the $BaTiO_3$ samples were sintered at temperatures higher than 1523 K, severe strain was observed as the melting temperature of the material (1898 K [PRADEEP]) was approached. Ceramic shrinkage, or pore reduction, is directly related to the initial particle size, as shown in Equation 2 [KINGERY]:

$$d - d_0 = (2k)^{1/2} t^{1/2} \quad (2)$$

where d and d_0 are the initial and final grain diameters, respectively, k is a constant, and t is the processing time. Sintering temperatures for the conventional route of ceramic preparation are reported to be between 1623 and 1703 K [ZHONG, WODECKADUS, TERANISHI]. The x-ray diffraction patterns of the thermally treated BSTx ceramics (Figure 11) clearly show the perovskite-type structure. As in the case of the powders, the peaks shift to higher angle as the Sr content increases. From Figure 12 it can be seen that the strongest peak shifts linearly (~0.1º) for each 0.1 increase in X (Sr content), and thus can be used to determine the sample composition (stoichiometry). Figure 13 plots the peak position as a function of the Sr content. All the thermally treated BSTx ceramics have the correct stoichiometry and present the perovskite-type structure ABO_3. However, the structure can be either tetragonal or cubic at room temperature depending on the processing conditions. For the $BaTiO_3$ the relative position of the (002) and (200) peaks determine the tetragonality of the phase, i.e., the ratio of the lattice parameters c/a. Such peaks appear at approximately $2\theta = 53°$.

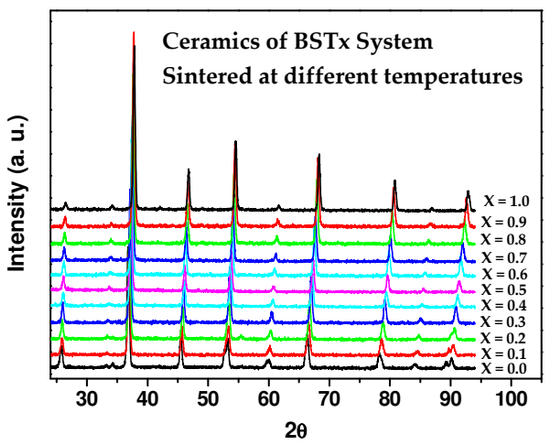

Fig. 11. X-ray diffraction patterns of BSTx ceramics system sintered from 1523 to 1573 K for 2h.

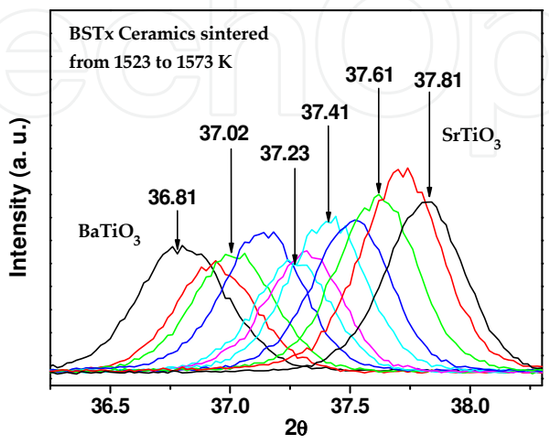

Fig. 12. Main XRD peaks of BSTx ceramic system sintered from 1523 to 1573 K of the figure 11.

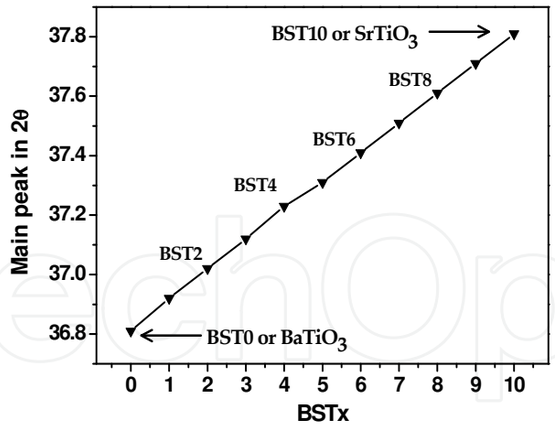

Fig. 13. Main diffraction peak position (Figure 12) as a function of stoichiometric composition.

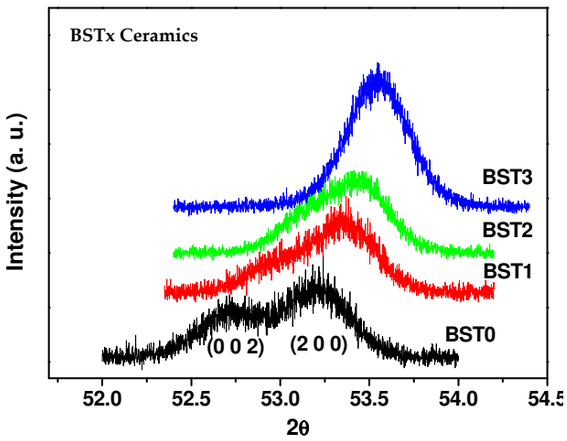

Fig. 14. Separation (or lack therof) of the (002) and (200) reflections of sintered ceramics BST0, BST1, BST2 and BST3 providing a measure of the c/a ration.

The phase is cubic and paralectric if the c/a ratio = 1. In such a case there is only a single peak near 2θ = 53°. If c/a > 1 the phase is tetragonal and ferroelectric. In such case there is a double peak. Figure 14 shows the BST0, BST1 and BST2 samples have a double peak, while sample BST3 apparently has only a single peak. Rietveld refinement (using Maud Program) was performed on the diffraction patterns of Figure 11 in order to determine the unit cell lattice parameters. The results, presented in Figure 15, show a gradual decrease in lattice parameters with increasing Sr content. This is due to the substitution of strontium Sr^{2+} ions (with ionic radius of 1.12 Å) for barium Ba^{2+} ions (with ionic radius of 1.34 Å). The tetragonality (c/a) decreases also from 1.008 (BST0) to 1.0014 (BST3) while for BST4 to BST10 it has value of 1. Differential scanning calorimetry (DSC), Raman spectroscopy, as well as the ferroelectric and dielectric measurements confirmed this phase transition, and are presented below, along with the cubic-to-tetragonal phase transition temperature (Curie temperature).

Ceramic Sample	Position in 2θ	Maximun intensity of the peak	Peak width	Lattice parameter of unit cell	Tetragonality c/a
BST0	52.694	704	0.485	a = 3.9953	1.0089
	53.227	1265	0.543	c = 4.0311	
BST1	52.942	388	0.520	a = 3.9844	1.0067
	53.368	1190	0.487	c = 4.0114	
BST2	53.124	490	0.446	a = 3.9785	1.0048
	53.459	1185	0.477	c = 3.9979	
BST3	53.457	1327	0.335	a = 3.9684	1.0014
	53.611	1764	0.360	c = 3.9737	
BST4	53.725	10	0.146	a = 3.9611	1

Table 2. Unit cell parameters and fitting parameters of peaks around 53° in 2θ.

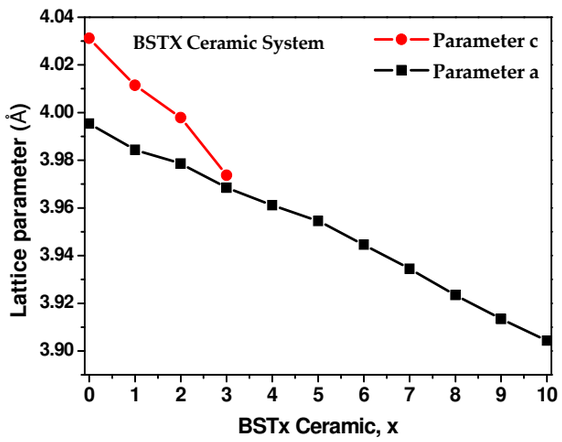

Fig. 15. Lattice parameter as a function of Sr content.

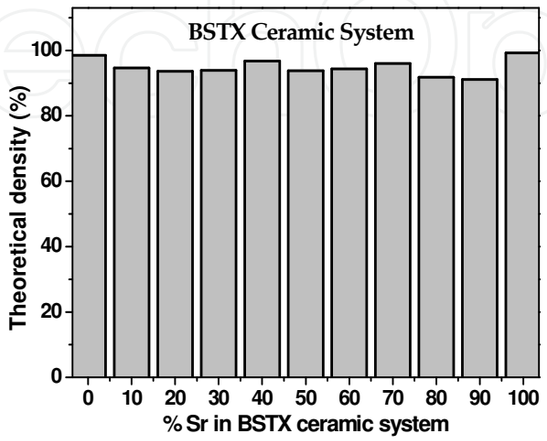

Fig. 16. Percentage of theoretical density of sintered compacts as a function of Sr content.

3.3 Density

With the actual volume of the unit cell and considering the number of barium, strontium, titanium and oxygen atoms composing the ABO_3 unit cell, the theoretical density can be calculated using:

$$\text{Theoretical Density} = \frac{\text{Unit cell mass}}{\text{Unit cell volume}} \tag{3}$$

The unit cell volume ($a^2 \times c$) was calculated using the results of the Rietveld analysis. The mass of the unit cell is calculated considering 3 oxygen, 1 titanium, (x) strontium and (1-x) barium atoms. The bulk density of the samples was determined by the Archimedes method. Figure 16 plots the bulk density as percentage of the theoretical density. All samples have bulk densities higher than 90% of theoretical, proving that the alternative fabrication route can attain a high densification of the ceramics. The density caluclation and measurment results are presented in Table 3.

BSTx Sample	Unit cell volume (Å^3)	Theoretical density (g m^{-3})	Bulk density (g m^{-3})	% Theoretical density
BST0	64.349	6.016	5.928	98.526
BST1	63.684	5.950	5.630	94.632
BST2	63.283	5.857	5.486	93.661
BST3	62.675	5.782	5.430	93.910
BST4	62.152	5.698	5.513	96.758
BST5	61.839	5.593	5.246	93.798
BST6	61.377	5.501	5.191	94.364
BST7	60.905	5.408	5.191	95.986
BST8	60.393	5.317	4.883	91.838
BST9	59.934	5.220	4.755	91.080
BST10	59.514	5.118	5.078	99.217

Table 3. Theoretical and bulk (measured) Densities of BSTx ceramic system.

SEM micrographs of transversely fractured sections from the BST0, BST4, BST8 and BST10 samples are shown in Figure 17. The BST0 ($BaTiO_3$) and BST10 ($SrTiO_3$) ceramics have a uniform compact morphology, present no cracks and have low porosity. The grain boundaries are not observable. Samples BST0 and BST10 have a bulk density of 98.52% and 99.21% of the theoretical, respectively. Even with the lower-than-conventional sintering temperatures, it is possible that the observed morphology resulted from liquid phase formation due to the small particle size [KINGERY, BARSOUM, BARRY]. Grain size distributions for BST0 and BST10 are shown in Figure 18. For the BST0 sample, grain sizes between 1 and 3.5 μm (2 μm average) were measured, while for the BST10 sample, sizes ranged ranged from 1 μm to 2.6 μm (1.4 μm average). The BST4 and BST8 samples, consisting of a barium-strontium solid solution $(Ba,Sr)TiO_3$, have a distinctly smaller grain size, with distributions of 0.2 to 1.3 μm (650 nm average) and 0.3 to 0.9 μm (550 nm average),

respectively. Generally speaking, the conventional route for fabrication of mixed oxide ceramics leads to grains larger than 1 μm, in most cases on the order of several microns [LIN, LIOU, LU]. Smaller grains are only attained with nanopowders and special sintering processes such as spark plasma sintering (SPS) [DENG] or hot pressing [XIAO]. Other methods for inhibiting grain growth include the incorporation of 1 wt% of Na, Mn or Mg ions [LIOU].

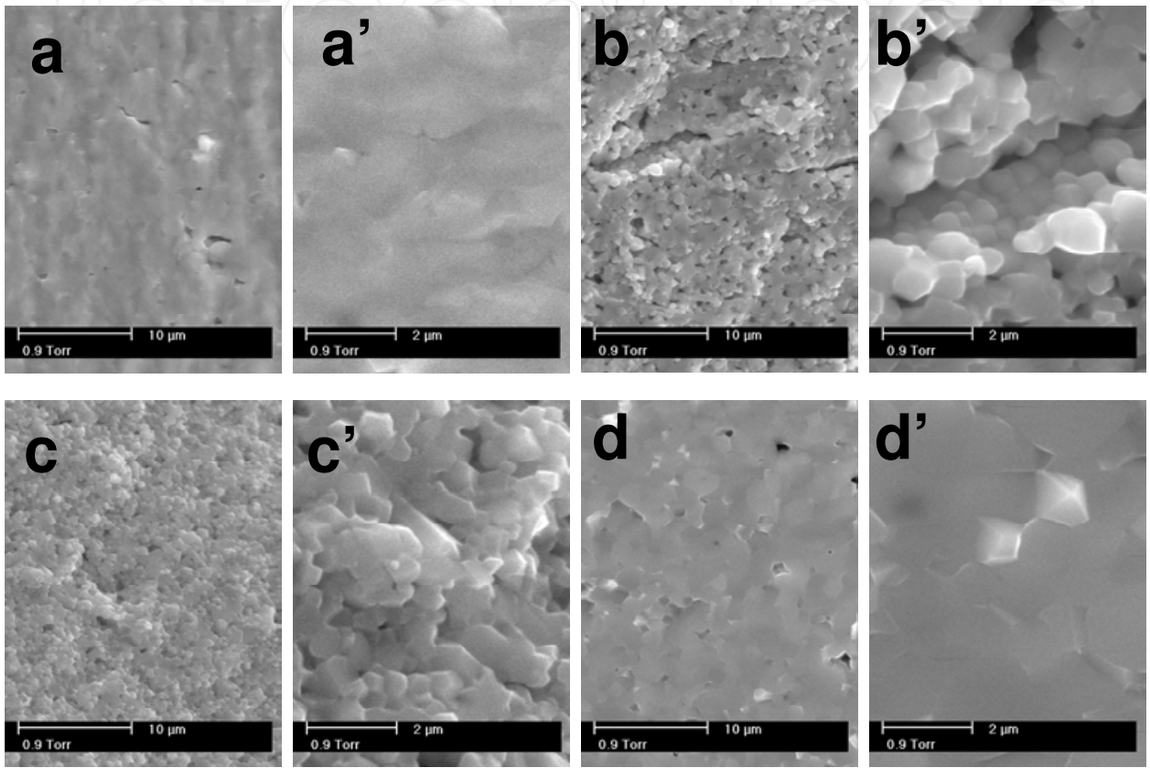

Fig. 17. SEM micrographs of transversely fractured BST0, BST4, BST8 and BST10 samples at two magnifications: (a) BST0 sintered at 1523 K, (b) BST4 sintered at 1543 K, (c) BST8 sintered at 1573 K, (d) BST10 sintered at 1573 K.

3.4 Curie temperature (Tc) via differential scanning calorimetry

DSC measurements were conducted from 203 to 423 K in a nitrogen atmosphere with a heating rate of 20°C/min. Figure 19 presents the DSC curves for samples BST0 to BST3. The cubic to tetragonal phase transition (Curie temperature, Tc) is an endothermic event. Tc decreases with increasing content of Sr in the samples, i.e., as the Sr^{2+} ions replace Ba^{2+} ions. This behavior was previously reported by Rupprecht and Bell [RUPPRECHET].

The linear dependence between the Tc and at.% Sr is described by Equation 4, the result of fitting the experimental data (Figure 20):

$$Tc = 128.4871 - 31.469*X \quad (4)$$

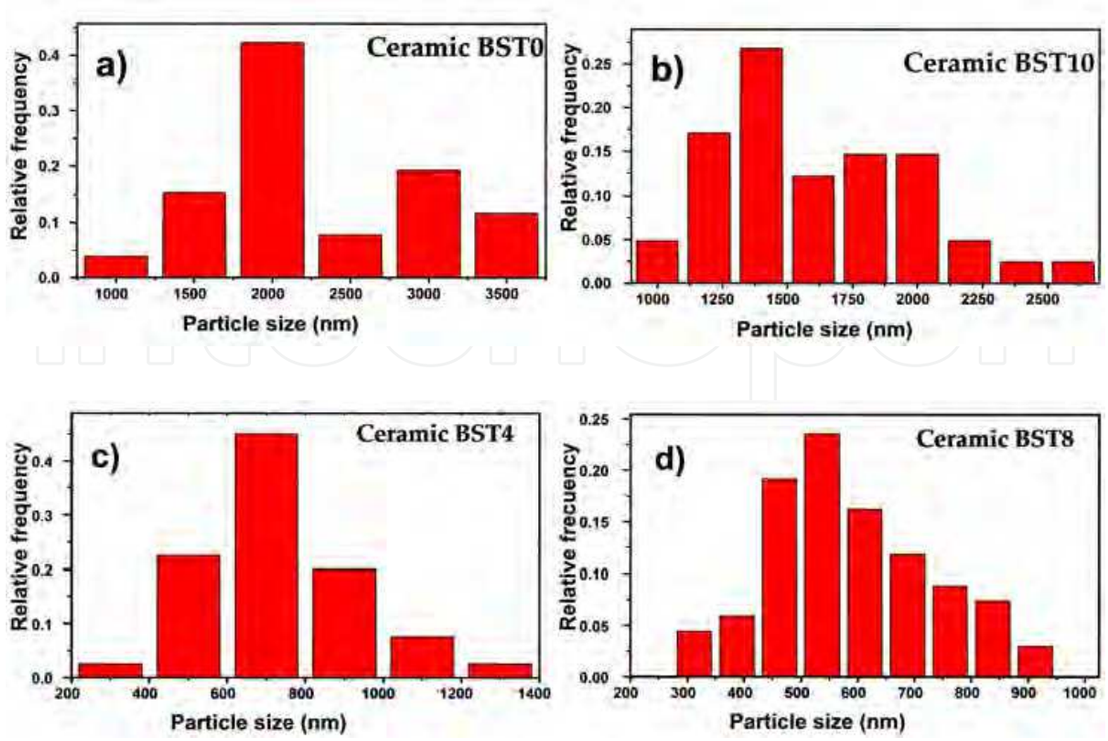

Fig. 18. Grain size distribution of (a) BST0, (b) BST10, (c) BST4 and (d) BST8 ceramic samples.

where Tc is the Curie temperature and x is the Sr content in at.%. Table 4 presents the Curie temperatures of samples BST0 to BST3 determined by Equation 4. The equation was extrapolated to the composition of samples BST4 to BST10. The determined Curie temperatures resulted not so different from those reported in the literature, for example, the BST35 system (35 mol% of Sr) has an approximate Tc of 292 K [ALI] compared to 291.35 K determined with Equation 4. The BST3 system was reported to have a Tc of 306~307 K [PITICESCU], compared to 307.08 K calculated with Equation 4. The $Ba_{60}Sr_{40}TiO_3$ system (BST4) has a Tc of 272 K (274.15 K) [FETEIRA], compared to our calculation of 276.6 K.

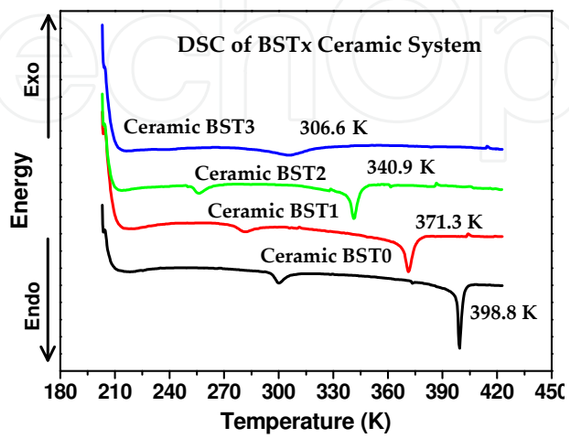

Fig. 19. Differential scanning calorimetry curves of the BST0, BST1, BST2 and BST3 samples.

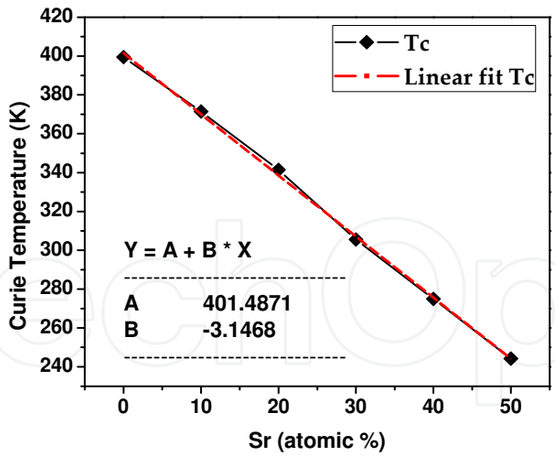

Fig. 20. Linear fit of the Curie temperature (Tc) from the DSC curves.

Sample ID	Calculated Tc (K)	Experimental Tc (K)
BST0	401.48	399.80
BST1	370.02	371.36
BST2	338.55	340.96
BST3	307.08	306.62
BST4	275.61	273.0
BST5	244.15	241.65
BST6*	212.68	
BST7*	181.21	
BST8*	149.74	
BST9*	118.27	
BST10*	86.80	

Table 4. Experimental Curie temperatures (via DSC), and those calculated using Equation 4. Tc for samples BST6 – BST10 were not experimentally determined due to exceeding the temperature range of the differential scanning calorimeter.

3.5 Curie temperature (Tc) via Raman spectroscopy

Figure 21 shows the Raman scattering spectrum (radiation wavelength = 514.5 nm) for $BaTiO_3$ (BST0) with perovskite-type structure ABO_3 and tetragonal phase at room temperature. Raman active phonons for the P4/mmm tetragonal symmetry are represented by 3A1 + B1 + 4E. Long-range electrostatic forces induce a splitting in the transverse and longitudinal phonons, resulting in a split of the Raman active phonons represented by 3 [A1 (TO) + A1 (LO)] + B1 + 4 [E (TO) + E (LO)] [SHIRATORI]. Raman shift bands are reported at 250, 520 and 720 cm^{-1} with a sharp peak at around 306 cm^{-1} [DIDOMENICO, ROUSSEAU, BASKARA].

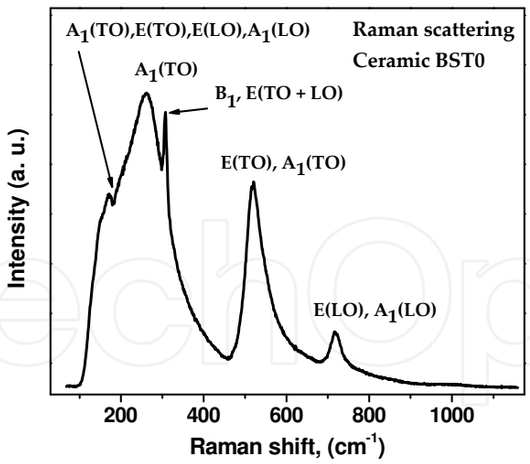

Fig. 21. Raman scattering spectra for BST0.

The shoulder at around 180 cm^{-1} in bulk $BaTiO_3$ is attributed to the coupling of the three disharmonic phonons A1 (TO) [VENKATESWARAN, FREY]. Figure 23 shows the Raman scattering spectra of the BST0 sample at different temperatures. The 250, 520 and 720 cm^{-1} bands as well as the 306 cm^{-1} peak decrease gradually as the temperature increases. At 403 K, the sharp 306 cm^{-1} peak disappears, indicating the transition from cubic to tetragonal phase (Tc). The transition temperature was previously reported by C. H. Perry [PERRY]. Thus, the sharp peak around 306 cm^{-1} indicates whether the BSTx system is in the tetragonal or cubic phase. The relative intensity of the 306 cm^{-1} peak as a function of temperature for BST0 is presented in Figure 22. Figures 24 and 25 show the temperature-dependent Raman scattering spectra for BST1 and BST2, respectively. The cubic to tetragonal phase transition is observed in the range from 363 to 373 K for BST1 and 333 to 343 K for BST2. Both ranges match those determined by DSC. Figure 26 shows the Raman scattering spectra for BST1 to BST5 at room temperature. Samples BST4 and BST5 do not present the sharp peak at 306 cm^{-1}, i.e., they have a stable cubic phase and a tetragonality of 1 (c/a = 1). These results are consistent the XRD and DSC results presented earlier.

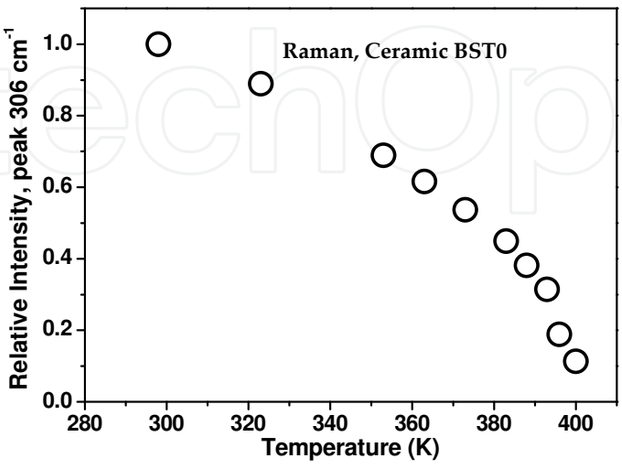

Fig. 22. Realtive peak intensity for the 306 cm^{-1} Raman reflection (from Figure 21) as a function of temperature for BST0.

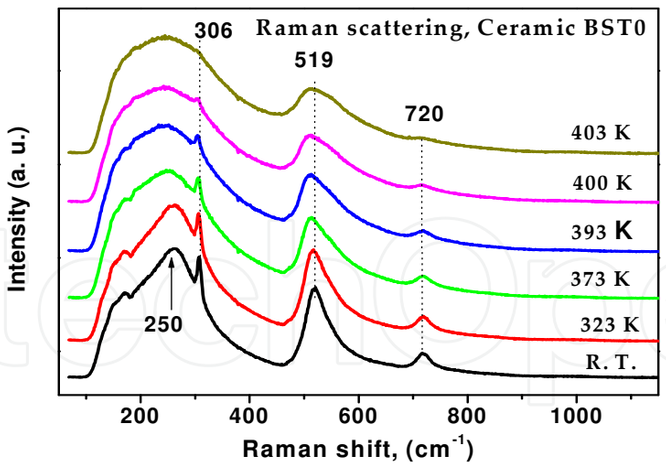

Fig. 23. Raman scattering spectra at different temperatures for BST0.

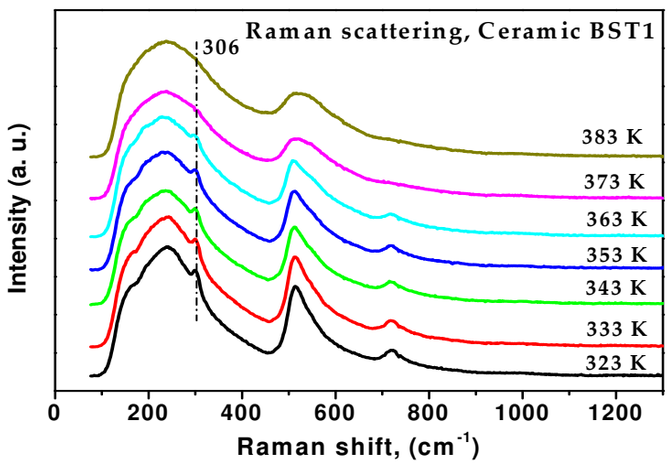

Fig. 24. Raman scattering spectra at different temperatures for BST1.

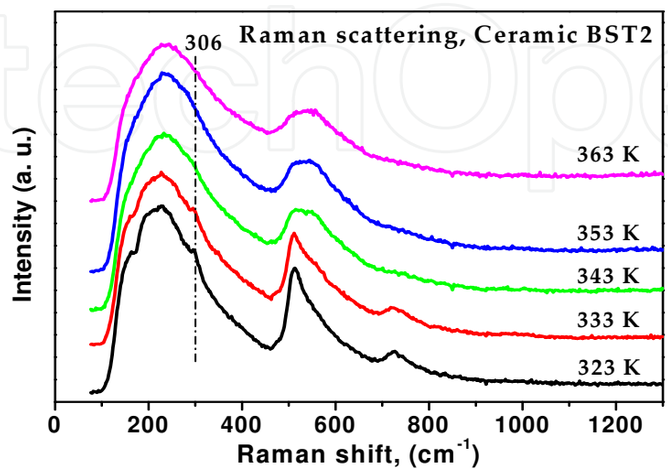

Fig. 25. Raman scattering spectra at different temperatures for BST2.

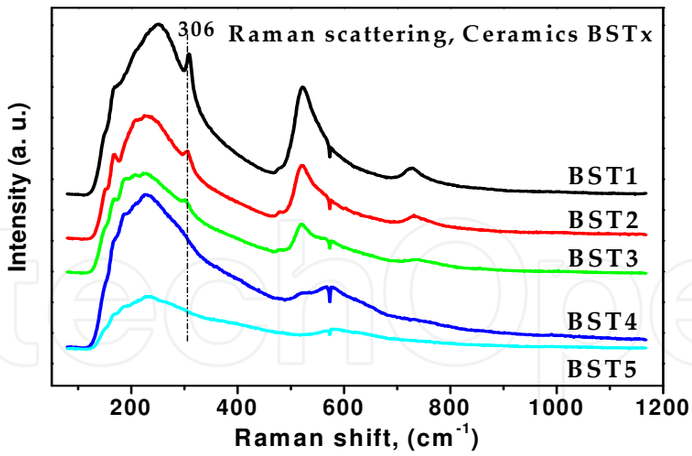

Fig. 26. Raman scattering spectra at room temperature for BST1, BST2, BST3, BST4 and BST5.

3.6 Dielectric and ferroelectric properties

3.6.1 Dielectric constant

When a polycrystalline ferroelectric ceramic is cooled below its Curie temperature, some of its properties undergo strong changes. For example, the dielectric constant (ε) shows a maximum at Tc for BST0, BST1 and BST3 at 0.1, 1.0, and 100 kHz (Figure 27), a typical ferroelectric behavior of perovskite-type materials [MILLAR, STANFORD]. A widening of the peak at Tc has been reported to occur with decreasing grain size [KINOSHITA, SAKABE]. The dielectric constant has a magnitude larger than 1000 within most of the measured temperature interval, and it decreases at higher frequencies. This effect has been observed in $BaTiO_3$ ceramics containing Zr [DEB] and in those containing Na and Bi (BTNx) [GAO]. The dielectric constant has polar and ionic parts, therefore, the dielectric dispersion can be attributed to the dipoles ceasing to contribute to the dielectric constant as the frequency increases [MERZ, 1954]. The dielectric relaxation effect occurs at frequencies where the electric dipoles can no longer follow the oscillation of the applied electric field. The relaxation frequency can be determined by a drop in the real part of ε and a maximum in the imaginary part [RAVEZ]. Although there is dielectric relaxation in the BSTx samples, the material does not present typical reflexor behavior. That is, there is no change in the position of Tc when the frequency changes. Another

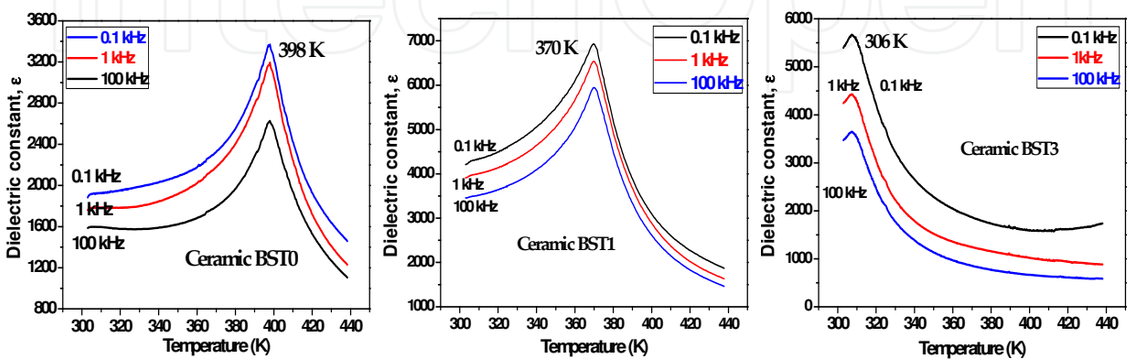

Fig. 27. Dielectric constant curves for (a) BST0, (b) BST1 and (c) BST3.

ferroelectric material with such a behavior is $Pb(Mg_{1/3}Nb_{2/3})O_3$ [KOVALA]. The determined Tc's agree well with those obtained by DSC and Raman. The dielectric constant peak values are 3.179, 6.540 and 4.432 for BST0, BST1 and BST3 ceramics respectively, 2 to 3 orders of magnitude larger than those of other materials conventionally used in capacitors or CMOS (complementary metal oxide semiconductor) devices [ROBERTO, WILK].

All of the BSTx samples showed a maximum in the dielectric constant at Tc. Above this temperature, the dielectric behavior obeys the Curie-Weiss law and has the form [BURFOOT]:

$$\varepsilon = \frac{C}{T - T_0} \tag{5}$$

where ε is the dielectric constant (material permittivity), C is the Curie-Weiss constant, T is the temperature of the material and T_0 is the Curie-Weiss temperature.

3.6.2 Ferroelectric hysteresis loops

When an external electric field ***E*** is applied to a dielectric material, it produces a ***P*** vs. ***E*** curve. In the case of ferroelectric materials there is a delay in the ***P*** response to the ***E*** stimulus, i.e., hysteresis. A freshly manufactured ferroelectric has a zero spontaneous net polarization ($\boldsymbol{P_s=0}$). When an external electric field is applied, nucleation and growth of the ferroelectric domains occur [MERZ, 1954].

The shape of the ferroelectric curve P = f(E) depends on both time and temperature. In the present work, ferroelectric measurements were performed at room temperature (~298 K) at a fixed frequency of 100 Hz using a comercial Sawyer-Tower circuit (ferroelectric RADIANT Test System) [SAWYER and TOWER]. Figure 28 presents the hysteresis loops for BST0, BST1, BST2 and BST3. The **P-E** urves exhibit the typical behavior of polycrystalline ferroelectric ceramics [MERZ, 1953]. The remanent polarization (P_r) is low compared to that of $BaTiO_3$ single crystals (>20 μC/cm² [SRIVASTAVA]), but higher than that of nanocrystalline $BaTiO_3$ (P_r < 1 μC/cm² [BUSCAGLIA]). It is comparable to that of $BaTiO_3$ ceramics with grain sizes of around 1 μm [TAKEUCHI].

3.7 Piezoresponse Force Microscopy (PFM)

3.7.1 Ferroelectric domain observation

Ferroelectric materials are composed of ferroelectric domains, which can be observed by polarized light microscopy [RUPPRECHT, ARLT], scanning electron microscopy [CHOU, ROUSSEAU] and transmission electron microscopy [FREY, GANPULE]. To be detected by these techniques, some sort of chemical attack is necessary to reveal the ferroelectric domains, as they demonstrate a preferential rate of erosion [FETEIRA, LAURELL]. Furthermore, these techniques do not directly indicate the direction of polarization (direction of the domain); they only discriminate one domain from another. Piezoresponse force microscopy (PFM) does not suffer from these shortcomings [RABE], allowing visualization of ferroelectric domains with sizes on the order of 1 μm [SAURENBACH, WITTBORN], accurate detection of the polarization direction [ENG 1998, CHO] and reconstruction of the three-dimensional orientation of the domains [ENG, 1999]. Figure 29 is a diagram of oriented domains in ferroelectric grains. Figure 29 (a shows a domain up and

one down (antiparallel ↑↓), separated by domain walls (gray stripe). The adjacent domains are oriented in opposite directions (180°). If these domains are observed from above, we would see that the direction of the domains are perpendicular to the surface, either pointing down into the sample (crosses) or up out of the sample (circles)., Both types are described as out-of-plane (OOP) (Figure 30). Figure 29 (b shows domains oriented at 90° (↑→) relative to one another. If these domains are observed from above, we would see domains in the plane of or parallel to the surface. These dominains are described as in-plane (IP) (Figure 30).

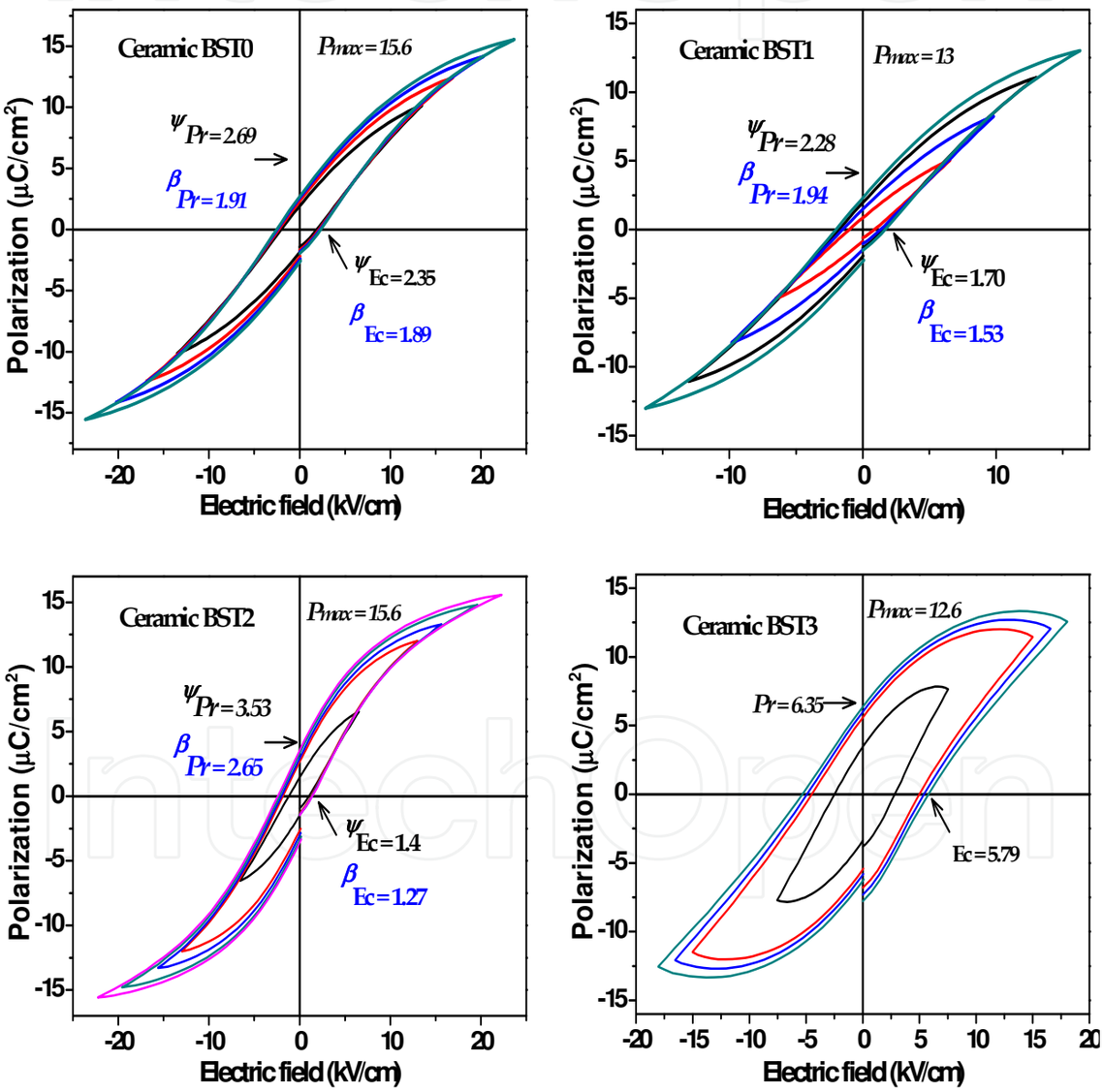

Fig. 28. P-E loops obtained for BST0, BST1, BST2 and BST3.

It isimportant to note that Figure 29 represents the ideal case of monocrystal domains ideally oriented, i.e., the direction of the observed polarization vectors are orthogonal. For the real case of a polycrystalline ceramic, the direction of the polarization vector would be random, i.e., a domain can point in any direction in 3D space. Therefore, the signals from piezoresponse measurements in OOP or IP are the projections of these random polarization vectors.

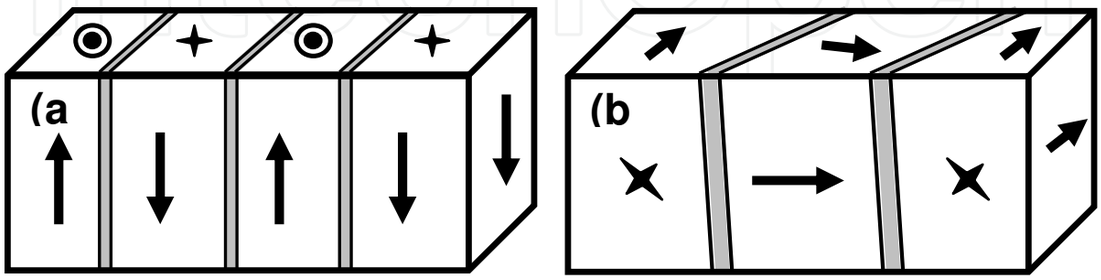

Fig. 29. Ferroelectric domains with differents orientations of the polarization vector. (a out-of-plane (OOP) and (b in-plane (IP).

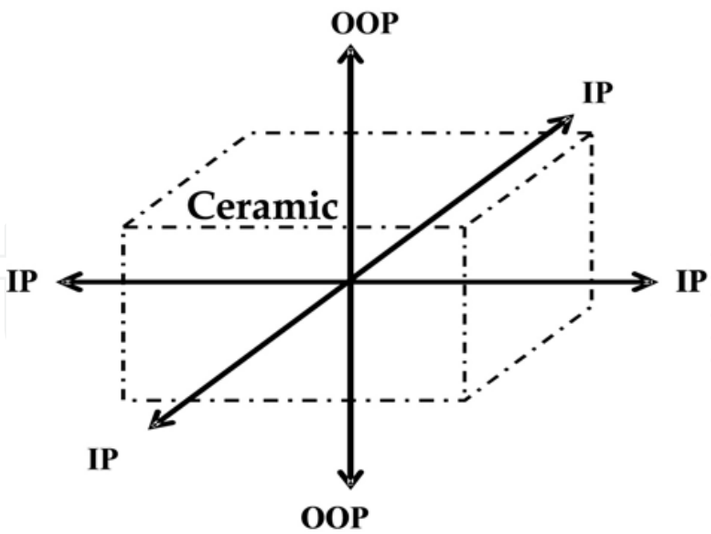

Fig. 30. Standard terminology for polarization vector orientations relative to the observed surface in piezoresponse force microscopy (PFM). IP refers to in-plane, and OOP is out-of-plane.

3.7.2 Contact Resonance-Enhanced Piezoresponse Force Microscopy (CR-PFM)

In addition to the conventional PFM technique there is another mode called contact resonance-enhanced PFM or CR-PFM [HARNAGEA]. R-PFM is based on the same principles of operation of as PFM, the only difference being the value of the frequency of the alternating voltage applied to the tip (V_{AC}). For contact resonance frequencies (CR-PFM), the strain amplitude response of the material can be more than one or two orders of magnitude higher than the amplitudes recorded by conventional PFM (quality factor Q) [HARNAGEA]. In other words, R-PFM is more sensitive than PFM and can be applied to materials whose piezoelectric constants (d_{ij}) are very small. Table 5 lists some materials and their piezoelectric constant (coefficient) .

Material	Piezoelectric coefficient, d_{33} (pm/V)
$Sr_{0.61}Ba_{0.39}Nb_2O_6$	200
$BaTiO_3$	190
PZT4	291
PZT5a	373
Quartz	3

Table 5. Piezoelectric constants of different materials.

The piezoelectric constant (d_{33}) indicates how much the material will be deformed (in picometers) for each applied volt (V) applied. or Fmaterials with a low piezoelectric constant, it would be necessary to amplify the piezoresponse signal by applying a high voltage, risking a change in piezoelectric response. In such cases, R-PFM is an alternative to observe ferroelectric domains while still using a low voltage.

3.7.3 Results of R-PFM for BSTx samples

R-PFM measurements for the BSTx samples were made using the modified conventional method on an atomic force microscope (AFM, Veeco di DimensionTM 3100), usig conductive tips of Cr/Pt (Budget Sensors Tap I300E) with a force constant k = 40 N/m, and a free-resonance frequency was 300 kHz. The samples were polished starting with No. 500 sandpaper down to 0.3 µm alumina. The samples were not attacked by any chemical or mechanochemical process, insuring that topography did not contribute to the piezoresponse signal. AFM images of the contact resonance mode piezoresponse (CR-PFM) for BST0, with a grain size of 1-2 µm, are shown Figure 31. The three images, taken of the same area and at the same time, show (a) the topography, (b) the OOP piezoresponse amplitude, and (c) the OOP piezoresponse phase. Measurements were performed over a 5 x 5 µm area, using an applied voltage was 2V and a contact resonance frequency of 1350

kHz. The amplitude and phase piezoresponse images present different characteristics. In the Figure 31b, the piezoresponse amplitude image allows us to visualize domains that leave or enter of the surface (OOP), where the amplitude *A* can be the same for antiparallel dominions (↑↓). Different regions are distinguished by their gray tones, delimited by black contours, which correspond to the ferroelectric domain walls. The domain walls are not observed in the topography, as that would have required etching (chemical attack) [FETEIRA]. Regions that appear as similar shades of gray in the piezoresponse amplitude image (Figure 31b) appear as contrasting bright and dark in the piezoresponse phase image (Figure 31c). This indicates a phase shift of 180˚ from one domain to another, but with the same piezoresponse amplitude.

These results show that the R-PFM images of amplitude and phase are not influenced by the topography of the samples. In contrast, standard measurements of piezoresponse force microscopy (PFM) were performed at 20 kHz with an alternating voltage (V_{ac}) of 2-15 V without obtaining a piezoelectric response. A piezoresponse was obtained with contact resonance frequencies (~1350 kHz), with a quality factor Q betwen 50 and 100. Taking into account both the quality factor Q and the piezoresponse signal reported about 190 pm/V and to 419 pm/V [SHAO] for the case of $BaTiO_3$, we can estimate a small piezoelectric constant of our material is of the order of units or tens of pm/V.

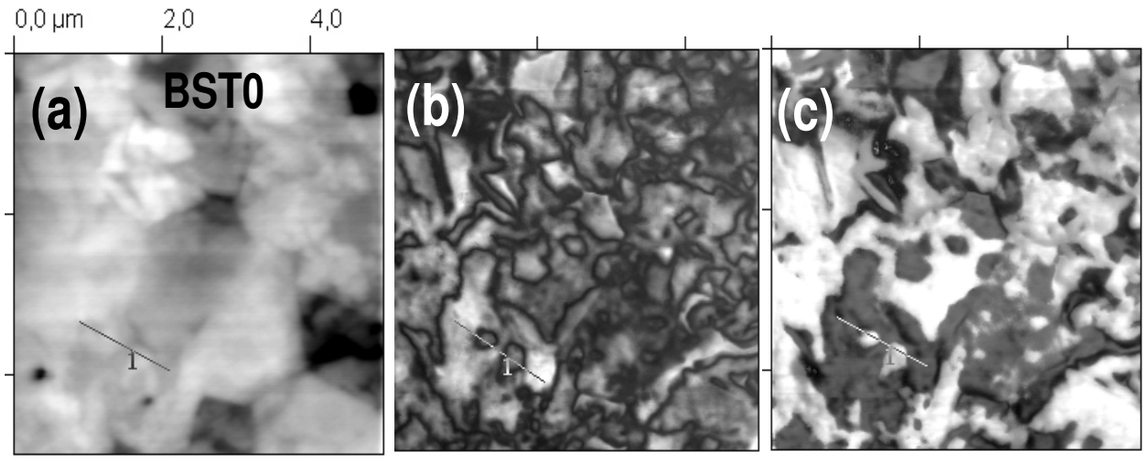

Fig. 31. R-PFM of BST0 at a frequency of 1.350 MHz and an excitation voltage of 2 V.
(a) topography, (b) piezorepsonse amplitude, and (c) piezoresponse phase.

4. Conclusion

The mixed oxides modified route (solid-state reaction) is a direct alternative to obtain highly densified BSTx ceramics. In this route, the high-energy ball milling and the applied heat treatment allowed the preparation of nanometric powders (less than 200nm) with Perovskite-type structure ABO_3. The Curie temperature of the BSTx ceramics was unambiguosly determined as a function of temperature by several techniques: Raman spectroscopy, differential scaning calorimetry, and measurements of dielectric constant. This temperature was succesfully tuned from 87 K to 400 K by varying the Sr/Ba ratio, as expected. However, a shifting in the orthorhombic to tetragonal phase transition was observed in the sintered ceramics. For instance, the OTPT for the BST0-BST2 samples was shifted down 17-27 K with respect to the literature. The origin of this shifting is probably residual stresses associated to the fine-grained microstructure of the sintered samples.

The group of BST0, BST1, BST2 and BST3 ceramics present P(E) curves with ferroelectric behavior at room temperature. The other cases present paraelectric behavior. Moreover, the BST0, BST1and BST2 samples present rather low maximum and remanent polarization and coercive fields. BSTx ceramics (x = 0, 1, 2, 3) displayed piezoelectric response in the contact resonance piezoresponse force microscopy mode (CR-PFM). The polycrystalline BSTx ceramics showed ferroelectric domains with sizes several times smaller than the grains.

5. Acknowledgment

This work was partially supported by CONACYT, Mexico. The authors would like to thank Michael Boldrick Ph. D. and Rodrigo Mayen Mondragón Ph. D. for their help regarding the english translation. Besides, we thank Pedro García J., J. Eleazar Urbina A., M. Adelaido Hernández L., Francisco Rodríguez M., Agustín Galindo S., Rivelino Flores F., Alfredo Muñoz S., Ma. del Carmen Delgado C. and Eduardo Larios for their technical aid.

6. References

Ali, N. J. & S. J. Milne, "Comparison of powder synthesis routes for fabricating $(Ba_{0.65}Sr_{0.35})TiO_3$ ceramics", *J. Mater. Res.*, 21 (2006) 1390-1398.

Arlt, G. & P. Saxo, "Domain configuration and equilibrium size of domain in $BaTiO_3$ ceramics", *J. Appl. Phys.*, 5 (1980) 4956-4960.

Asiaie, R.; Weidong Zhu, Sheikh A. Akbar, & Prabir K. Dutta, "Characterization of submicron particles of tetragonal $BaTiO_3$", *Chem. Mater.*, 8 (1996) 226-234.

Baláz, P. & B. Plesingerova, "Thermal properties of mechanochemically pretreated precursors of $BaTiO_3$ synthesis", *J. Therm. Anal. Cal.*, 59 (2000) 1017-1021.

Barry C. (2007). "Ceramic Material Science and Engineering", Springer, USA.

Barsoum M. W. (2003). "FUNDAMENTALS OF CERAMICS", McGraw, USA.

Baskara, N.; Anil Hule, Chutan Bhongale, Ramaswamy Murugan & Hua Chang, "Phase transition studies of ceramic $BaTiO_3$ using thermo-Raman and dielectric constant measurement", *J. Appl. Phys.*, 91 (2002) 10038-10043.

Berbecaru, C.; H. V. Alexandru, C. Porosnicu, A. Velea, A. Ioachim, L. Nedelcu & M. Toacsan, "Ceramic materials $Ba_{(1-x)}Sr_xTiO_3$ for electronics — Synthesis and characterization", Thin *Solid Films*, 2008, 516, (22), 8210–8214.

Blomqvist, M.; Sergey Khartsev & Alex Grishin "Electrooptic ferroelectric $Na_{0.5}K_{0.5}NbO_3$ films", *IEEE Photonics Technology Letters*, 17 (2005) 1638-1640.

Boland, S. W.; Suresh C. Pillai, Weing-Duo Yang & Sossina M. Haile, "Preparation of (Pb,Ba)TiO_3 powders and highly oriented thin films by a sol-gel process", *J. Mater. Res.*, 19 (2004) 1492-1498.

Burfoot. Jack C. "*Ferroelectrics*", D. Van Nostrand Company LTD, London.

Buscaglia, M. T.; Massimo Viviani, Vincenzo Buscaglia, Liliana Mitoseriu, Andrea Testino, Paolo Nanni, Zhe Zhao, Mats Nygren, Catalin Harnagea, Daniele Piazza, & Carmen Galassi, "High dielectric constant and frozen macroscopic polarization in dense nanocrystalline $BaTiO_3$ ceramics", *Phys. Rev. B*, 73 (2006) 064114.

Busch, G. & P. Scherrer, *Naturwiss*, 23 (1935) 737.

Chaisan W.; S. Ananta & T. Tunkasiri, "Synthesis of barium titanate-lead zirconate solid solution by a modified mixed-oxide synthetic route", *Curr. Appl. Phys.*, 4 (2004) 182-185.

Chen, Chin-Yen & Hur-Lon Lin, "Piezoelectric properties of $Pb(Mn_{1/3}Nb_{2/3})O_3$-$PbZrO_3$-$PbTiO_3$ ceramics with sintering aid of $2CaO$-FeO_2 compound", *Ceram. Int.*, 30 (2004) 2075-2079.

Cheng, H.; Jiming Ma & Zhenguo Zhao, "Hydrothermal synthesis of PbO-TiO_2 solid solution", *Chem. Mater.*, 6 (1994) 1033-1040.

Cho, Y.; Satoshi Kazuta & Kaori Matsuura, "Scanning nonlinear dielectric with nanometer resolution", *Appl. Phys. Lett.*, 75 (1999) 2833-2834.

Chou, Jung-Fang, Ming-Hong Lin & Hong-Yang Lu, "Ferroelectric domains in pressureless-sintered barium titanate", *Acta Mater.*, 48(2000) 3569.

Deb, K. K.; M. D. Hill & J. F. Nelly, "Pyroelectric characteristics of modified barium titanate ceramics", *J. Mater. Res.*, 7 (1992) 3296-3304.

Deng, X.; Xiaohui Wang, Hai Wen, Liangliang Chen, Lei Chen, & Longtu Li, "Ferroelectric properties of nanocrystalline barium titanate ceramics", *Appl. Phys. Lett.*, 88 (2006) 252905.

DiDomenico, M.; Jr., S. P. S. Porto, S.H. Wemple & R. P. Barman, "Raman spectrum of single-domain $BaTiO_3$", *Phys. Rev.*, 174 (1968) 522-530.

Ding, Z.; R. L. Frost & J. T. Kloprogge, "Thermal Activation of Cooper Carbonate", *J. Mater. Sci. Lett.*, 21 (2002) 981-983.

Eng, L. M., H.; –J. Güntherodt, G. A. Schneider, U. Köpe & J. Muñoz Saldaña, "Nanoscale reconstruction of surface crystallography from three-dimensional polarization distribution in ferroelectric barium-titanate ceramics", *Appl. Phys. Lett.*, 74 (1999) 233-235.

Eng, L. M.; H. –J. Güntherodt, G. Rosenman, A. Skilar, M. Oron, M Katz and D. Eger, "Nondestructive imaging & characterization of ferroelectric domains in periodically poled cristal", *J. Appl. Phys.*, 83 (1998) 5973-5977.

Feteira, A.; Derek C. Sinclair, Ian M. Reaney, Yoshitaka Somiya, & Michael T. Lanagan, "$BaTiO_3$-Based Ceramics for Tunable Microwave Applications", *J. Am. Ceram. Soc.*, 87 (2004) 1082-1087.

Frey, M. H. & D. A. Payne, "Grain-size effect on structure and phase transformations for barium titanate ", *Phys. Rev. B*, 54 (1996) 3158-3167.

Frey, M. H. & D. A. Payne, "Grain-size effect on structure and phase transformations for barium titanate", *Phys. Rev. B*, 54 (1996) 3158-3168.

Ganpule, C. S., V. Nagarajan, B. K. Hill, A. L. Roytburd, E. D. Williams & R. Armes, "Imaging three-dimensional polarization in epitaxial polydomain ferroelectric thin films", J. *Appl. Phys.*, 91 (2002) 1477-1481.

Gao, L.; Yanqiu Huang, Yan Hu & Hongyan Du, "Dielectric and ferroelectric properties of (1-x)$BaTiO_3$-x$Bi_{0.5}Na_{0.5}TiO_3$ ceramics", *Ceram. Int.*, 33 (2007) 1041-1046.

Gopalan, V. & Terence E. Mitchell, "Wall velocities, switching times, and the stabilization mechanism of 180° domains in congruent $LiTaO_3$ crystals", *J. Appl. Phys.*, 83 (1998) 941-954.

Gururaja T. R; Walter A. Schulze, Leslie E. Cross, Robert E. Newnham, Bertram A. Auld & Yuzhong J. Wang, "Piezoelectric Composite Materials for Ultrasonic Transducer Applications", *IEEE*, 32 (1985) 481-498.

Hammer, J. M. "Digital electro-optic grating deflector and modulator", *Appl. Phys. Lett.*, 18 (1971) 147-149.

Harnagea, C.; Alain Pignolet, Marin Alexe & Dietrich Hesse, "Higher-Order Electrochemical Response of Thin Films by Contact Resonant Piezoresponse Force Microscopy", *IEEE*, 53 (2006) 2309-2321.

Hidaka T.; T. Maruyama, M Saitoh & N. Mikoshiba, "Formation and observation of 50 nm polarized domains in $PbZr_{1-x}Ti_xO_3$ thin film using scanning probe microscope", *Appl. Phys. Lett.*, 68 (1996) 2358-2359.

Ianculescu, A.; A. Brăileanu & Georgeta Voicu, "Synthesis, microstructure and dielectric properties of antimony-doped strontium titanate ceramics", *J. Eur. Ceram. Soc.*, 27 (2007) 1123-1127.

Judd, M. D. & M. I. Pope, "Energy of activation for the decomposition of the alkaline-earth carbonates from thermogravimetric data", *J. Therm. Anal.*, 4 (1972) 31-38.

Kamalasanan, M. N.; N. Deepal Kumar & Subhas Chandra, "Structural and microstructural evolution of barium titanate thin films deposited by the sol-gel process", *J. Appl. Phys.*, 76 (1994) 4603-4609.

Kingery. (1960). "Introduction to Ceramics", Second Ed., John Wiley & Sons, USA.

Kingon, A.; "Is the ultimate memory in sight?", *Nat. Mater.*, 5 (2006) 251-252.

Kingon, Angus I,; Jon-Paul Maria & S. K. Streiffer, "Alternative dielectrics to silicon dioxide for memory and logic devices", *Nature*, 406 (2000) 1032-1038.

Kinoshita Kyoichi & Akihiko Yamaji, "Grain-size Effects On Dielectric Properties in Barium Titanate Ceramics", *J. Appl. Phys.*, 47 (1976) 371-373.

Kohlstedt, H.; Y. Mustafa, A. Gerber, A. Petraru, M. Fitsilis, R. Meyer, U. Böttger & R Waser, "Current status and chellenges of ferroelectric memory devices", *Microelectronic Engineering*, 80 (2005) 296-304.

Kong, L. B.; J. Ma, H. Huang, R.F. Zhang & W.X. Que, "Barium titanate derived from mechanochemically actived powders" *J. Alloys Compd.*, 337 (2002) 226-230.

Kotecki, D. E.; "(Ba,Sr)TiO_3 dielectrics for future stacked capacitors DRAM", *IBM J. Res. Develop.*, 43 (1999) 367-380.

Kovala, V.; Carlos Alemany, Jaroslav Briancin, Helena Bruncková & Karol Saksl, "Effect of PMN modification on structure and electrical response of xPMN-(1-x)PZT ceramic systems", *J. Eur. Ceram. Soc.*, 23 (2003) 1157-1166.

Kugel, V. D.; G Rosenman & D. Shur, "Electron emission from $LiNbO_3$ crystals with domains of inverted polarization", *J. Phys. D: Appl. Phys.*, 28 (1995) 2360-2364.

L'vov, Boris V. & Valery L. Ugolkov, "Peculiarities of $CaCO_3$, $SrCO_3$ and $BaCO_3$ decomposition in CO_2 as a proof of their primary dissociative evaporation", *Thermochim. Acta*, 410 (2004) 47-55.

Laurell, F.; M. G. Roelofs, W. Bindloss, H. Hsiung, A Suna and J. D. Bierlein, "Detection of ferroelectric domain reversal in $KTiOPO_4$", *J. Appl. Phys.*, 71 (1992) 4664-4670.

Lin, Ming-Hong; Jung-Fang Chou & Hong-Yang Lu, "Grain-Growth Inhibition in Na2O-Doped TiO_2-Excess Barium Titanate Ceramic", *J. Am. Ceram. Soc.*, 83 (2000) 2155-2162.

Liou, Jih_Wei & d Bi-Shiou Chiou, "Effect of Direct-Current Biasing on the Dielectric Properties of Barium Strontium Titanate", *J. Am. Ceram. Soc.*, 80 (1997) 3093-3099.

Liou, Jing-Kai; Ming-Hong Lin & Hong-Yang Lu, "Crystallographic Facetting in Sintered Barium Titanate", *J. Am. Ceram. Soc.*, 85 (2002) 2931-2937.

Lu, Chung-Hsin; Wei-Hsing Tuan & Buh-Kuan Fang, "Effects of Pre-sintering Heat Treatment on the Microstructure of Barium Titanate", *J. Mater. Sci. Lett.*, 15 (1996) 43-45.

Masui, S.; Shunsuke Fueki, Koichi Masuntani, Amane Inoue, Toshiyuki Teramoto, Tetsuo Suzuki & Shoichiro Kawashima, "The Application of FeRAM to Future Information Technology World", *Topics Appl. Phys.*, 93 (2004) 271-284.

Merz Walter J. "Double Hysteresis Loop of $BaTiO_3$ at the Curie Point", *Phys. Rev.*, 91 (1953) 513-514.

Merz, Walter J. "Domain formation and Domain Wall Motions in Ferroelectric $BaTiO_3$ Single Crystal", *Phys. Rev.*, 95 (1954) 690-698.

Meschke, F.; A. Kolleck & G. A. Schneider, "R-curve behaviour of $BaTiO_3$ due to stress-induced ferroelastic domain switching", *J. Eur. Ceram. Soc.*, 17 (1997) 1143-1149.

Millar C. A. "Hysteresis Loss and Dielectric Constant in Barium Titanate", *Brit. J. Appl. Phys.*, 18 (1967) 1689-1697.

Padmaja, G.; Ashok K. Batra, James R. Curie, Mohan D. Aggarwal, Mohammad A. Alim & Ravindra B. Lal "Pyroelectric ceramics for infrared detection applications", *Mater. Lett.*, 60 (2006) 1937-1942.

Park, Yong-I, "Effect of composition on ferroelectric properties of sol-gel derived lead bismuth titanate ($PbBi_4Ti_4O_{15}$) thi films", *J. Mater. Sci.*, 36 (2001) 1261-1269.

Perry, C. H. & D. B. Hall, "Temperature Dependence of the Raman Spectrum of the $BaTiO_3$", *Phys. Rev. Lett.*, 15 (1965) 700-702

Piticescu, R. M.; P. Vilarnho, L. M. Popescu, R. R. Piticescu, "Hydrothermal synthesis of perovskite based materials for microelectronic applications", *J. Optoelectron. Adv. Mater.*, 8 (2006) 543-547.

Pradeep, P. P.; Subhash H. & Risbud, "Low-temperature synthesis and processing of electronic materials in the BaO-TiO_2 system", *J. Mater. Sci.*, 25 (1990) 1169-1183.

Rabe, U.; M. Kopycinska, S. Hirsekorn, J. Muñoz Saldaña, G. A. Schneider & W. Arnold, "High-resolution characterization of piezoelectric ceramics by ultrasonic scanning force microscopy techniques", *J. Phys. D: Appl. Phys.*, 35 (2002) 2621-2635.

Radheshyam, R. & Seema Sharma, "Structural and dielectric propierties of Sb-doped PLZT ceramics", *Ceram. Int.*, 30 (2004) 1295-1299.

Ravez, J. "Ferroelectricity in Solid State Chemistry", *Chem.*, 3 (2000) 267-283.

Razak, K. A.; A. Asadov & W. Gao, "Properties of BST prepared by high temperature hydrothermal process", *Ceram. Int.*, 33 (2007) 1495-1502.

Relva, B. C. (2004). "Ceramic Materials for Electronics", Marcel Dekker, USA.

Roberto, J. "High Dielectric Constant Oxides", *Eur. Phys. J. Appl. Phys.*, 28 (2004) 265–291.

Rosenman, G.; A. Skliar & I. Lareah, "Observation of ferroelectric domain structures by secondary-electron microscopy in as-grown $KTiOPO_4$ crystals", *Phys. Rev. B*, 54 (1996) 6222-6226.

Rousseau, D. L. & S. P. S. Porto, "Auger-like Resonant Interference in Raman Scattering From One and Two-Phonon States of $BaTiO_3$", *Phys. Rev. Lett.*, 20 (1968) 1354-1357.

Rupprecht, G. & R. O. Bell, "Microwave Losses in Strontium Titanate above the Phase Transition", *Phys. Rev.*, 125 (1962) 1915-1920.

S. Maitra, N. Chakrabarty & J. Pramanik, "Decomposition kinetics of alkaline heart carbonates by integral approximation method", *Ceramica*, 54 (2008) 268-272.

Sakabe, Y.; N. Wada & Y. Hamaji, "Grain Size Effects on Dielectric Properties and Crystal Structure of Fine-grained $BaTiO_3$ Ceramics", *J. Korean Phys. Soc.*, 32 (1998) 260-264.

Sato, H. & Kohji Toda, "An Application of $Pb(Zr,Ti)O_3$ Ceramic to Opto-Electronic Devices", *Appl. Phys.*, 13 (1977) 25-28.

Saurenbach, F. & B. D. Terris, "Imaging of ferroelectric domain walls by force microscopy", *Appl. Phys. Lett.*, 56 (1990) 1703-1705.

Sawyer, B. & C. H. Tower, "Salt rochelle as a dielectric", *Phys. Rev.*, 35 (1930) 269-273.

Shao, S.; Jialiang Zhang, Zong Zhang, Peng Zheng, Minglei Zhao, Jichao Li1 & Chunlei Wang, "High piezoelectric properties and domain configuration in $BaTiO_3$ ceramics obtained through the solid-state reaction route", *J. Phys. D: Appl. Phys.*, 41 (2008) 125408 (5pp).

Shepard, R. "Dielectric and Piezoelectric Properties of Barium Titanate", *Phys. Rev.*, 71 (1947) 890-895.

Shiratori, Y.; C. Pithan, J. Dornseiffer & R. Waser, "Raman scattering studies on nanocrystalline $BaTiO_3$ Part II – consolidated polycrystalline ceramics", *J. Raman Spectrosc.*, (2007).

Srivastava, N. & G.J. Weng, "The influence of a compressive stress on the nonlinear response of ferroelectric crystals", *Int. J. Plas.*, 23 (2007) 1860-1873.

Stanford, A. L. "Dielectric resonance in Ferroelectric Titanates in the Microwave Region", *Phys. Rev.*, 124 (1961) 408-410.

Takashi Teranishi, Takuya Oshina, Hiroaki Takeda & Takaaki Tsurimi, "Polarization behavior in diffuse phase transition of $Ba_xSr_{1-x}TiO_3$ ceramics", *J. Appl. Phys.*, 105 (2009) 054111.

Takeuchi, T.; Claudio Capiglia, NaliniBalakrishnan, Yasuo Takeda & Hiroyuki Kageyama, "Preparation of fine-grained $BaTiO_3$ ceramics by spark plasma sintering", *J. Mater. Res.*, 17 (2002) 575-581.

Uchino, Kenji. (2000). "Ferroelectric Devices", Marcel Dekker, USA.

Valasek, J. "Piezo-Electric And Allied Phenomena In Rochelle Salt", *Phys. Rev.*, 17 (1921) 475-481.

Venkateswaran, UD.; Naik VM & Naik R, "High-pressure Raman studies of polycrystalline $BaTiO_3$ ", *Phys. Rev. B*, 58 (1998) 14256.

Vittayakorn, N.; Theerachai Bongkarn & Gobwute Rujijanagul, "Phase transition, mechanical, dielectric and piezoelectric properties of Perovskite $(Pb_{1-x}Ba_x)ZrO_3$ ceramics", *Physica B*, 387 (2007) 415-420.

Vold, R. E.; R. Biederman, G. A. Rossettu JR., & A. Sacco JR., "Hydrothermal synthesis of lead doped barium titanate", *J. Mater. Sci.*, 36 (2001) 2019-2026.

Wainer, E. & A. N. Salomon, Titanium Alloy Manufacturing Company Elect. Rep. 8 (1942), 9 and 10 (1943).

Whatmore, R. W.; Qi Zhang, Christopher P. Shaw, Robert A. Dorey & Jeffery R. Alcock, "Pyroelectric ceramics and thin films for applications in uncooled infra-red sensor arrays", *Phys. Scr. T.*, 129 (2007) 6-11.

Wilk, G. D.; R. M. Wallace & J. M. Anthony, "High-k Gate Dielectrics: Current Status and Materials Properties Considerations", *Appl. Phys. Rev.*, 89 (2001) 5243-5275.

Wittborn. J.; C. Canalias, K. V. Rao, R. Clemens, H. Karlsson & F. Laurell, "Nanoscale imaging of domain and domain walls in periodically poled ferroelectrics using atomic force microscopy", *Appl. Phys. Lett.*, 80 (2002) 1622-1624.

Wodecka-Dus, B.; A. Lisinska-Cekaj. T. Orkisz, M. Adamczyk, K. Osinska, L. Kozielski & D. Czekaj, "The sol-gel synthesis of barium strontium titanate ceramics", *Mater. Sci. Poland*, 25 (2007) 791-799.

Xiao, C. J.; W. W. Zhang, Z. H. Chi, F. Y. Li, S. M. Feng, C. Q. Jin, X. H. Wang, L. T. Li, & R. Z. Chen, "Ferroelectric $BaTiO_3$ nanoceramics prepared by a three-step high-pressure sintering method", *Phys. Stat. Sol.*, 204 (2007) 874-880.

Xu, H. & Lian Gao, "Hydrothermal sinthesis of high-purity $BaTiO_3$ powders: control of powder and size, sintering density, and dielectric properties", *Mater. Lett.*, 58 (2004) 1582-1586.

Yamashita, Kouchi Harada, Yasuharu Hosono, Shinya Natsume & Noboru Ichinose, "Effects of B-site Ions on the Electrochemical Coupling Factors of $(Pb(B'B'')O_3$-$PbTiO_3$ Piezoelectric Materials", *Jpn. J. Appl. Phys.*, 37 (1998) 5288-5291.

Yamashita, Y.; Yasuharu Hosono & Noboru Ichinose, "Phase Stability, Dielectrcis and Peizoelectric Properties of the $Pb(Sc_{1/2}Nb_{1/2})O_3$-$Pb(Zn_{1/3}Nb_{2/3})O_3$-$PbTiO_3$", *Jpn. J. Appl. Phys.*, 36 (1997) 1141-1145.

Yoo, J. H.; W. Gao & K. H. Yoon, "Pyroelectric and dielectric bolometer properties of Sr modified $BaTiO_3$ ceramics", *J. Mater. Sci.*, 34 (1999) 5361-5369.

Yun, S. N.; X. L. Wang & D. L. Xu, "Influence of processing parameters on the structure and properties of barium strontium titanate ceramics", *Mater. Res. Bull.*, 2008, 43, (8–9), 1989–1995.

Zhi, Y.; Ruyan Guo, A.S. Bhalla, "Dielectric polarization and strain behavior of $Ba(Ti_{0.92}Zr_{0.08})O_3$ single crystal", *Mater. Lett.*, 57 (2002) 349-354.

Zhong, Z. & Patrick K. Gallagher, "Combustion synthesis and characterization of $BaTiO_3$", *J. Mater. Res.*, 10 (1995) 945-952.

Zhu, M.; Lei Hou, Yudong Hou, Jingbing Liu, Hao Wang & Hui Yan, "Lead-free $(K_{0.5}Bi_{0.5})TiO_3$ powders and ceramics prepared by sol-gel method", *Mater. Chem. Phys.*, 99 (2006) 329-332.

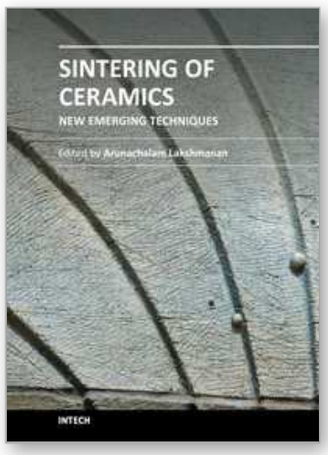

Sintering of Ceramics - New Emerging Techniques
Edited by Dr. Arunachalam Lakshmanan

ISBN 978-953-51-0017-1
Hard cover, 610 pages
Publisher InTech
Published online 02, March, 2012
Published in print edition March, 2012

The chapters covered in this book include emerging new techniques on sintering. Major experts in this field contributed to this book and presented their research. Topics covered in this publication include Spark plasma sintering, Magnetic Pulsed compaction, Low Temperature Co-fired Ceramic technology for the preparation of 3-dimesinal circuits, Microwave sintering of thermistor ceramics, Synthesis of Bio-compatible ceramics, Sintering of Rare Earth Doped Bismuth Titanate Ceramics prepared by Soft Combustion, nanostructured ceramics, alternative solid-state reaction routes yielding densified bulk ceramics and nanopowders, Sintering of intermetallic superconductors such as MgB2, impurity doping in luminescence phosphors synthesized using soft techniques, etc. Other advanced sintering techniques such as radiation thermal sintering for the manufacture of thin film solid oxide fuel cells are also described.

InTech Europe
University Campus STeP Ri
Slavka Krautzeka 83/A
51000 Rijeka, Croatia
Phone: +385 (51) 770 447
Fax: +385 (51) 686 166
www.intechopen.com

InTech China
Unit 405, Office Block, Hotel Equatorial Shanghai
No.65, Yan An Road (West), Shanghai, 200040, China
中国上海市延安西路65号上海国际贵都大饭店办公楼405单元
Phone: +86-21-62489820
Fax: +86-21-62489821

IntechOpen